Available online at www.sciencedirect.com
SCIENCE DIRECT®
Colloids and Surfaces B: Biointerfaces 42 (2005) 29–43
COLLOIDS AND SURFACES B
www.elsevier.com/locate/colsurfb

Surface modification of surface sol–gel derived titanium oxide films by self-assembled monolayers (SAMs) and non-specific protein adsorption studies

Maria Advincula[a], Xiaowu Fan[b], Jack Lemons[a], Rigoberto Advincula[a,b,c,*]

[a] *Department of Biomedical Engineering, University of Alabama at Birmingham, Birmingham, AL 35294, USA*
[b] *Materials Science Program, University of Alabama at Birmingham, Birmingham, AL 35294, USA*
[c] *Department of Chemistry, University of Houston, Houston, TX 77204, USA*

Received 11 October 2004; received in revised form 2 December 2004; accepted 17 December 2004

Abstract

Biological events occurring at the implant–host interface, including protein adsorption are mainly influenced by surface properties of the implant. Titanium alloys, one of the most widely used implants, has shown good biocompatibility primarily through its surface oxide. In this study, a surface sol–gel process based on the surface reaction of metal alkoxides with a hydroxylated surface was used to prepare ultrathin titanium oxide (TiO_x) coatings on silicon wafers. The oxide deposited on the surface was then modified by self-assembled monolayers (SAMs) of silanes with different functional groups. Interesting surface morphology trends and protein adhesion properties of the modified titanium oxide surfaces were observed as studied by non-specific protein binding of serum albumin. The surface properties were investigated systematically using water contact angle, ellipsometry, X-ray photoelectron spectroscopy (XPS), and atomic force microscopy (AFM) measurements. Results showed that the surface sol–gel process predominantly formed homogeneous, but rough and porous titanium oxide layers. The protein adsorption was dependent primarily on the silane chemistry, packing of the alkyl chains (extent of van der Waals interaction), morphology (porosity and roughness), and wettability of the sol–gel oxide. Comparison was made with a thermally evaporated TiO_x–Ti/Si-wafer substrate (control). This method further extends the functionalization of surface sol–gel derived TiO_x layers for possible titanium alloy bioimplant surface modification.

1. Introduction

The adsorption of proteins at the implant–tissue interface is the first event known to occur when a foreign material is introduced to the body, e.g. it is of central importance to the osseointegration process. Among these proteins, fibronectin and vitronectin, which contain the polyacidic sequence Arg–Gly–Asp (RGD) recognized by cell-surface integrin receptors, are believed to be the primary glycoproteins in serum that promote cell adhesion. Integrin-mediated cell adhesion then initiates a cascade of events that promote several structural changes in cells including spreading and cytoskeletal organization which then modulate longer-term events such as protein production [1]. Albumin, on the other hand, is the most abundant protein component of serum. It functions as a carrier protein for a range of small molecules, lipids, etc., and is important in maintaining balance between the extracellular and interstitial fluid compartments of the body. It has high affinity for titanium and its non-specific adsorption to the surface inhibits osteoblast cell adhesion in vitro [2,3].

Since biological tissues have been known to interact with mainly the outermost atomic layers of an implant [4], the surface oxide properties of the implant play an important role in protein adsorption. Specifically, surface chemistry, topography, roughness and wettability can affect the type, quantity and conformation of an adsorbed protein layer. For instance, serum albumin has been shown to absorb on smooth titanium

* Corresponding author. Tel.: +1 713 7431760; fax: +1 713 7431755.
E-mail address: radvincula@uh.edu (R. Advincula).

0927-7765/$ – see front matter © 2004 Elsevier B.V. All rights reserved.
doi:10.1016/j.colsurfb.2004.12.009

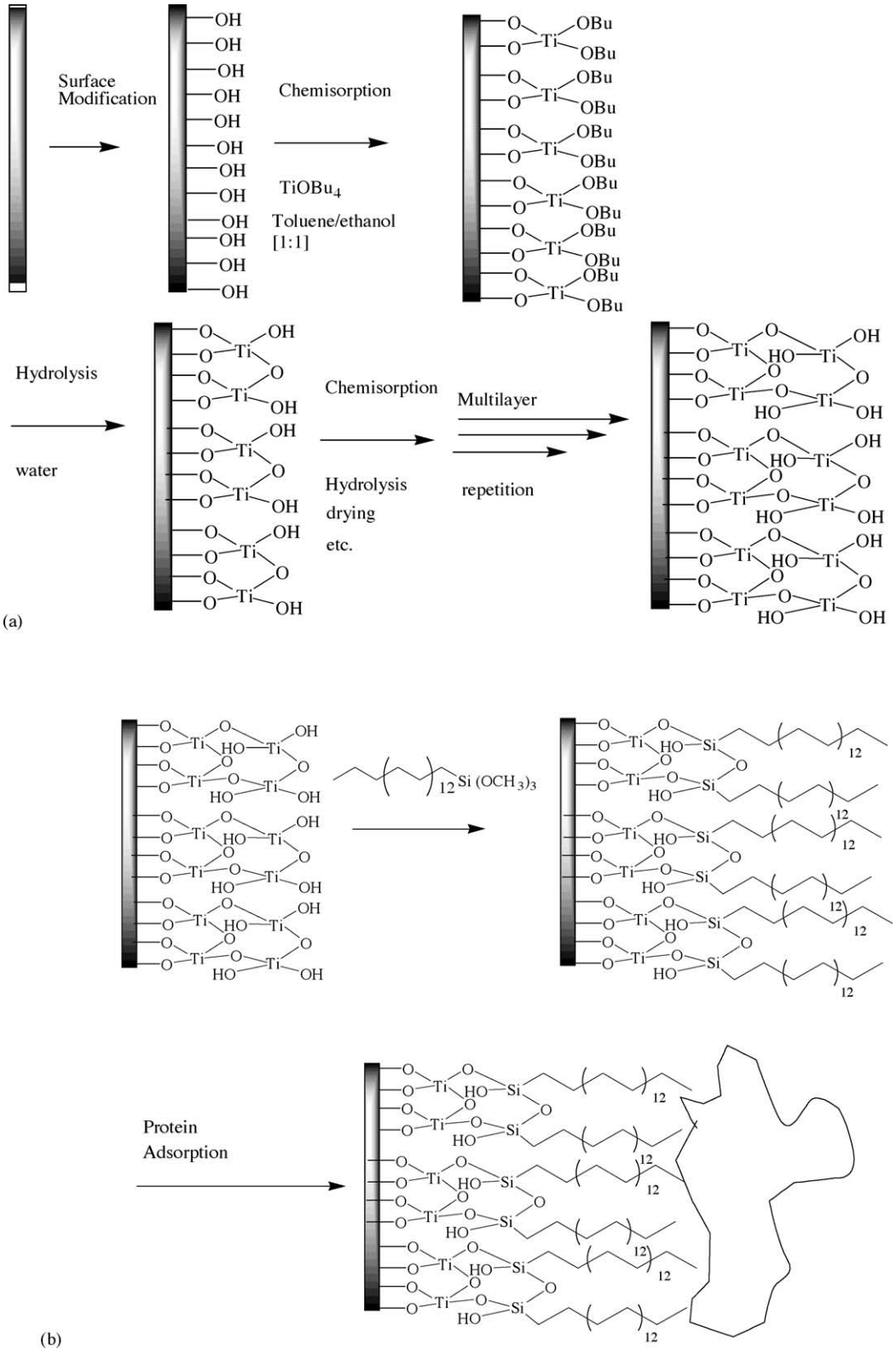

Fig. 1. The schematic diagrams describe: (a) the surface modification and surface sol–gel layer-by-layer deposition process on a substrate surface. The reaction on the formation of TiO_x bonds is usually facilitated by heating; (b) the self-assembled monolayer (SAM) modification on a TiO_x film prepared by the surface sol–gel layer-by-layer deposition process on a substrate surface.

surfaces in contrast to serum fibronectin which was adsorbed preferentially on rougher titanium surfaces [5]. Depending on the chemistry, different serum ligands are adsorbed on patterned surfaces which affect both cell adhesion and mineralization in vitro [6]. More integrins and osteoblast precursor cells bind to hydroxylapatite than titanium or steel due to adsorption of serum proteins in suitable conformations [7]. Thus, protein adsorption may be regulated by controlling the surface properties of an implant material.

Current modification techniques for promoting protein adsorption or activating the surface of common biomaterials such as titanium focus on altering the microstructure, chemistry, and wettability of the surface. These include, acid or chemical treatment, plasma treatment, chemical vapor deposition, thermal vacuum deposition, polymerization, formation of self-assembled monolayers (SAMs), etc. [8–10]. Activation of surfaces by SAMs is based on the strong adhesion of alkanethiols or alkylsilanes for gold or glass [10–12]. Since titanium and titanium alloy surfaces exist in their oxidized state, SAMS can readily form on the oxidized titanium by silane binding to yield surfaces with greater stability and functionality. Supramolecular architectures of biomolecules have been fabricated using SAMs for biosensors, bioactive coatings, host–guest templates, micropatterned supports, etc. [10,12,13]. Reactive functional groups (−PO_4, −COOH, −OH, etc.) immobilized on silane modified surfaces affect important cell behavior as cell spreading, migration and cytoskeletal organization, adsorption of protein, and nucleation of biomimetic calcium apatite layer [14–18].

The sol–gel technique is a wet chemical process that can be used to coat substrates with metal oxides. By combining SAMs and the sol–gel process, the surface properties of titanium alloys can be controlled to produce a more bioactive surface, i.e. promote cell and protein adhesion. Surface sol–gel processing or SSP is a relatively new sol–gel preparation that produces ultrathin titanium oxides with nanometer precision [19–22]. This process is based on the stepwise adsorption (chemisorption) of metal alkoxide on a hydroxylated substrate, rinsing, subsequent hydrolysis to regenerate the hydroxylated surface, and drying. The procedure can be repeated several times to produce the desired thickness of the oxide and each sol–gel process is independent of the other which allows each layer to be nanostructured [19].

In this paper, we would like to describe our investigation on the surface properties of sol–gel derived ultrathin TiO_x layers that is further modified by SAMs and their in vitro protein adsorption behavior (Fig. 1a and b). To our knowledge, there have been only limited studies on modifying sol–gel derived TiO_x with self-assembled monolayers (SAMs). The morphology and nanoporosity of these oxide films influences the SAM formation as well as the subsequent adhesion properties of proteins. Comparison to idealized SAMs formed on thermal vacuum evaporated TiO_x films on flat Si-wafers were made in relation to surface activity. Thus, this study is useful in investigating the fouling or non-fouling of surface oxide films derived from this stepwise sol–gel processing method and its subsequent application to biomedical implant devices.

2. Materials and methods

2.1. Substrates and coating

Silicon wafers of prime grade, resistivity 0.00600 Ω, thickness 500 μm (Wafernet Inc., San Jose, CA) were cut into small rectangular pieces (1 in. × 1 in.), cleaned with acetone to remove the debris and soaked in *Piranha* solution (30:70 vol.% mixture of 30 wt.% hydrogen peroxide and 98 wt.% sulfuric acid) for 30 min to form well-defined surface hydroxyl (oxide)layers. The samples were thoroughly rinsed and sonicated 3× with deionized or DI water (resistivity = 18.2 MΩ, and pH = 6.82, Millipore Inc.). Thin titanium oxide (TiO_x) was formed on the surface using a sol–gel technique developed by Kunitake et al. [15]. Briefly, the wafers were immersed in 10 mM solution of titanium alkoxide (Aldrich, Milwaukee, WI) in 1:1 toluene (Aldrich) and ethanol (Pharmco, Brookfield, CT) for 5 min in a sealed slide-staining jar deaerated with N_2 gas since the titanium butoxide is highly moisture sensitive. The titanium alkoxide reacted with the negatively charged hydroxyl groups on the surface during this chemisorption process. After rinsing with copious solvent to remove unbound alkoxides, the samples were immersed in de-ionized (DI) water for 1 min to regenerate the hydroxyl groups and then dried by N_2 gas. Chemisorption, rinsing, hydrolysis and drying were repeated for five cycles. The formation of the TiO_x bonds can also be facilitated by heating. For this experiment, the films were not heated in order to obtain the amorphous form of the oxide film. A schematic diagram of the procedure is shown in Fig. 1a.

For control, silicon wafers coated with 260 nm titanium layer (with native oxide) by vacuum thermal evaporation, were obtained from Spire Biomedical Inc (Bedford, MA) for parallel protein adsorption studies. The surface was passivated using 40% nitric acid and then placed under a plasma cleaner (PLASSMOD, March Instruments Inc., Concord, CA) in argon atmosphere for 350 s and dehydrated at 120 °C for 24 h to clean the surface and promote a fresh native oxide layer growth in air. This was further treated with piranha solution to hydroxylate the surface for coupling with the silane reagents. These samples will also be referred to as "control TiO_x or TiO_x–Ti/Si-wafer" samples.

2.2. Silanization

The samples were immersed in silane toluene solutions consisting of trialkoxy derivatives for 24 h. Tridecafluoro-1,1,2,2-tetrahydrooctyl) triethoxysilane is a straight chain alkane terminated by an ethoxide (hydrophobic), 2-hydroxy-4-(3-triethoxysilylpropoxy)-diphenylketone is a carbonyl-group containing alkane (hydrophilic-polar), octadecyltrimethoxysilane has a long alkyl chain (hydrophobic),

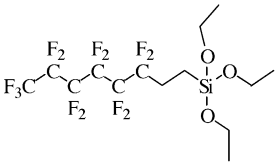

(Tridecafluoro-1,1,2,2-tetrahydro-octyl) triethoxysilane

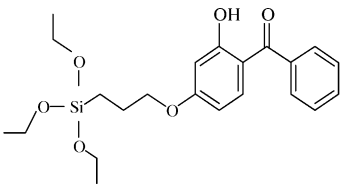

2-hydroxy-4-(3-triethoxysilylpropoxy)-diphenylketone

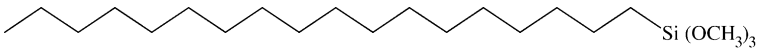

Octadecyltrimethoxysilane

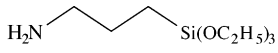

3-amino-propyltriethoxy-silane

Fig. 2. Chemical structures of the silane agents use for SAM formation on the TiO_x layers.

3-amino-propyltriethoxy-silane is a widely used coupling agent with an amino terminal group (hydrophilic). All silanes were purchased from Aldrich (Milwaukee, WI) and used as received. Fig. 2 shows the chemical representation of the different silanes. The substrates were rinsed with toluene, acetone then DI water each time for 10 min then dried with N_2. The silanization process was done in triplicates for each silane group.

2.3. Protein adsorption studies

Protein adsorption studies were done in vitro to investigate non-specific protein binding of albumin. A 0.01 M phosphate buffer saline (PBS) solution was prepared using a protocol described elsewhere [14]. Bovine serum albumin (BSA), a commonly used serum protein, was dissolved in PBS in a 1 mg/ml concentration. The substrates were immersed in 70% ethanol for 10 min, rinsed 3× in PBS to rehydrate the surface then immersed in protein solution for 24 h until adsorption was complete. The samples were removed from the solution, rinsed with PBS 3× and with DI water to remove unbound proteins and salt residues. Surface properties were immediately analyzed and the protein surface coverage was calculated based on the formula given below [14]:

$$\Gamma = d_{\text{dry protein}}\rho_0 = d_{\text{native protein}}\frac{1 - 1/N^2_{\text{native protein}}}{1 - 1/N^2_{\text{dry protein}}}\rho_0$$

$$= Kd_{\text{native protein}}(\text{ng/mm}^2)$$

where d is the thickness of protein layer, ρ the protein density, $\rho_0 \sim 1.37\ \text{g/cm}^3$, N the refractive index, $N_{\text{native protein}} \sim 1.465$ and $N_{\text{dry protein}} \sim 1.55$, $K \sim 1.2 \times 10^6\ \text{ng/mm}^3$. The values used were in accordance with previous studies using ellipsometry to measure the surface coverage of adsorbed serum albumin [14,23].

2.4. Surface characterization

2.4.1. Ellipsometry

A Multiskop ellipsometer (Optrel GmbH, Berlin, Germany) with 632.8 nm He–Ne laser as the light source was used to measure the optical thickness of metal oxides and protein layers. Software integrated in the instrument was used to calculate the ellipsometric angles, Δ (delta) and ψ (psi) of the polarized light beam reflected on the surface. The thickness of the layer formed was determined using a computer model fit of these parameters and the optical constants of the layer (e.g. silicon oxide, titanium oxide and native protein) [6,15,16]. Assuming that the monolayer formed remains stable as the thickness increases, the ellipsometric characterization model is built from a two-phase (ambient/silicon wafer), to three-phase (ambient/sol–gel TiO_x film/silicon wafer), to four-phase model (ambient/protein film/sol–gel TiO_x/silicon wafer), and finally, the thickness of the monolayer is subtracted from the bulk layer model. The ellipsometric model is shown in Table 1. Three points on each sample were measured and averaged.

2.4.2. Water contact angle

Surface wettability of the substrates was determined by the half angle method using a CAM-MICRO model contact angle meter (Tantec Inc., Schaumburg, IL). Deionized water was

Table 1
Ellipsometric layer model for the determination of the thickness (given the refractive index constants) on the modified films and the subsequent adsorption of proteins

Medium	n (refractive index)	k (extinction coefficient)	d (thickness)
0, Air	1	0	–
1, BSA	1.465	0	measured
2, Silanes	1.5	0	measured
3, TiO_2	2.5045/1.65	0	measured
Ti/Si	2.17/1.4598	−2.94/0	–

used as probe liquid. For static contact angle measurements, three spots were measured on each sample and averaged. Three samples for each group were used.

2.4.3. AFM

Atomic force microscopy (AFM) images of the multilayers morphology were obtained using a PicoScan system (Molecular Imaging, Phoenix, AZ) equipped with a 7 μm × 7 μm scanner. All images were collected at magnetic alternating current (MAC®) mode in air. The AFM tip consisted of a MAC lever® which is a silicon nitride-based cantilever coated with magnetic film. The force constant of the tip was around 0.5 N/m and the resonance frequency was around 100 kHz. The average roughness represented by the root mean square (rms) roughness of the surface was calculated based on a standard formula integrated in the imaging software.

2.4.4. SEM

A Philips XL30 SEM was used to obtain secondary electron images at primary beam energies of 10–15 kV. Typical sampling depth was a few microns.

2.4.5. XPS

The surface composition and chemistry were analyzed using X-ray photoelectron spectroscopy (XPS) (Kratos Axis 165) with a multitechnique electron spectrometer. A nonmonochromatic Al Kα X-ray source at 15 kV and 20 mA initiated the photoelectron emission. Using the Fixed Analyzer Transmission (FAT) mode, survey scans were collected from 0 to 1400 eV. The samples were measured over a spot area of 800 μm × 200 μm with resolution 4 eV and analyzer pass energy of 160 eV. The binding energy reference was the C 1s peak of hydrocarbon signal (284.5 eV).

2.5. Statistical analysis

Statistical analysis was done using one-way ANOVA. Mean difference based on $p = <0.05$ was considered significant.

3. Results and discussion

An important consideration of this investigation was to determine the effects of SAM silanization on the wettability and morphology of sol–gel derived TiO_x and on the in vitro behavior of protein adsorption. The SAM modification allowed variable surface energies and intermolecular forces of attraction for immobilization of proteins. The adsorption of proteins on surfaces involves several stages, i.e. adsorption, lateral mobility, dissociation, denaturation, irreversible adsorption, and exchange of protein with solution. By comparing with a control (vacuum evaporated TiO_x–Ti), a contrast on the surface energy, morphology, and porosity of the sol–gel TiO_x can be made.

Table 2
Water contact angle in degrees

	TiO_x–sol–gel on SiO_x–Si-wafer mean (S.D.)	Control–evaporated TiO_x–Ti/Si-wafer mean (S.D.)
After Piranha-solution (TiO_x)	34 (2)	20 (2)
After sol–gel	46 (5)	–
$-CF_3$	78 (9)	98 (2)
$-CH_3$	91 (2)	101 (2)
$-NH_2$	67 (6)	49 (3)
Benzophenone	81 (4)	76 (3)

3.1. Wettability by contact angle measurements

The water contact angle measurement data are shown in Table 2. In the first stage, the piranha solution treated evaporated TiO_x–Ti/Si-wafer substrates (control) and TiO_x sol–gel–SiO_x/Si-wafer showed very low contact angles due to formation of surface hydroxyl groups. After sol–gel deposition (five layers), the contact angles of the latter substrate increased. After silanization with the various SAMs, the samples then had different hydrophobicities, demonstrated by the contact angle differences (i.e. more hydrophobic = higher contact angles) resulting from various functional groups on silanes. In general, all contact angles increased after the SAM procedure. Sample ($-NH_2$) had the lowest (most hydrophilic) contact angle, while samples ($-CH_3$), ($-CF_3$) and benzophenone having the highest (most hydrophobic) contact angles. There was no significant difference between these latter groups ($p > 0.05$). For the TiO_x-evaporated substrates (control), the lowest (most hydrophilic) was also sample ($-NH_2$). Both samples ($-CF_3$) and ($-CH_3$) have higher contact angles ($p = 0.985$), and therefore, the most hydrophobic. The contact angles of sample ($-NH_2$) for both control and sol–gel substrates were similar ($p = 0.747$).

From these data several things can be noted. First of all, the results showed that the sol–gel TiO_x process increases the contact angle compared to the native oxide of the TiO_x–Ti/Si-wafer control. The contact angles increased further after SAM silanization indicating a general trend towards decreased wettability (hydrophobicity) by the SAM modification process, with the exception of the ($-NH_2$). The contact angles and thickness are consistent with the silane organic functionality and packing of alkyl chains, e.g. more hydrophobic, higher contact angle and lower contact angle, more hydrophilic. The higher contact angles for the hydrophobic SAMs and the lower contact angle for the hydrophilic SAM on the control TiO_x, indicates that these oxides are closer to ideal SAM chemisorption and packing behavior [24].

3.2. Ellipsometric thickness

Thickness data by ellipsometry are shown in Table 3. The TiO_x thickness on the Ti coated SiO_x/Si-wafers (before any treatment) ranged from 2 to 3 nm. After piranha solution treatment, the thickness remained relatively the same, around

Table 3
Thickness in nm by Ellipsometry

	TiO_x–sol–gel on SiO_x–Si-wafer mean (S.D.)	Control–evaporated TiO_x–Ti/Si-wafer mean (S.D.)
As received (TiO_x/SiO_x)	1.8 (0.2)	2.9 (0.2)
Acid treatment (TiO_x)	2.1 (0.2)	4.3 (0.3)
After sol–gel (TiO_x)	4.7 (0.4)	–
$-CF_3$	1.55 (0.27)	0.62 (0.13)
$-CH_3$	2.20 (1.33)	1.63 (0.10)
$-NH_2$	1.17 (0.16)	2.22 (0.07)
Benzophenone	2.05 (0.74)	1.52 (0.16)

2–4 nm. After sol–gel coating, the TiO_x oxide thickness increased on the SiO_x/Si-wafer, which was higher compared to the oxide formed on evaporated TiO_x–Ti/Si-wafer. The two different set of substrates were then modified by SAMs. For the sol–gel TiO_x, relatively higher silane SAM thicknesses were found in samples ($-CH_3$), ($-CF_3$) and benzophenone ($p > 0.05$) compared to the sample ($-NH_2$). For the control TiO_x substrates, the thickest silane layers were found on samples ($-CH_3$), benzophenone, and ($-NH_2$) ($p > 0.05$) though and the least thickness on sample ($-CF_3$). These trends are interesting and maybe related to the difference in the SAM formation process between the two oxide surfaces. It is also interesting to note that the thickness of the SAMs for the sol–gel derived TiO_x substrates are similar to the control TiO_x with the exception of the ($-NH_2$), which is higher for the control ($p < 0.05$). The quality of the SAM is dependent on both the effective surface area (roughness or flatness of substrate) and density of –OH groups for silanization, assuming the same silane crosslinking mechanism [24].

In general, the thickness data is consistent with the dimensions of the SAM agents but the rms roughness (by AFM) indicated the absence of homogeneity in the submicron area range. In addition, silane molecules with longer alkyl chains ($-CH_3$) or bigger polar groups (benzophenone) were deposited with a higher density on the sol–gel TiO_x (by comparison of area and thickness). The increased adsorption of sample ($-CH_3$) on sol–gel could be due to the increased alkyl chain (van der Waals forces) or hydrophobic interactions. Sample benzophenone silane contains carbonyl groups which can interact with the hydroxyl groups of the sol–gel. Variations in thickness as the layers are deposited can also be attributed to changes in growth morphology, growth mechanism or orientation during the SAM formation process [24–26]. For the sol–gel derived TiO_x, the silane layers are thicker than the reported values based on reaction-site limited monolayers [21]. The average thickness of the TiO_x deposited after five dipping cycles is approximately 5 nm. This also approximates the native oxide thickness of most air oxidized Ti metal surfaces. However, the sol–gel layers, gives a more porous morphology with higher rms roughness. This is observed in the two different morphologies between the sol–gel and control TiO_x substrates by AFM. The films increased in roughness and became even less uniform after deposition of the different silanes. This is expected as the sol–gel and native oxide surfaces can interact with the silanes depending on the silane chemistry, packing of alkyl chains, hydrophobicity and roughness. It could also be due to the higher surface area afforded by a sol–gel morphology. The heterogeneity of a sol–gel derived oxide has been shown to increase or decrease with deposition of SAMs or polymers [13].

3.3. AFM measurements

The surface of the sol–gel TiO_x and the evaporated control TiO_x has different morphologies as revealed by AFM. This contributes to the difference in thickness of the SAM silanes and also the surface energy. The sol–gel derived TiO_x has much smaller spherical domains and edgy features consistent with a more amorphous topology (Fig. 3). On the other hand, the thermally evaporated control TiO_x–Ti/Si-wafer substrates formed more regular and globular domains. In addition, SEM image of TiO_x–sol–gel–Ti/Si-wafer surface showed a flat, rough and porous film of finite thickness (not shown). For the SAMs deposited on the sol–gel TiO_x layers, homogeneous spherical domains were observed on ($-NH_2$) while a more patchy dense surface topography was observed on benzophenone (both hydrophilic samples). Higher packing density of molecules is seen on samples ($-CF_3$) and ($-CH_3$) which are the more hydrophobic SAMs. For the control TiO_x ($-NH_2$) had a uniformly dense surface while samples ($-CF_3$), benzophenone, ($-CH_3$) showed no obvious differences. All the surface morphologies after the silane deposition of the different SAMs are shown in Figs. 4 and 5. By AFM, it is possible to determine the mean roughness of the morphological features within a given area. The rms roughness of the surface was 1.5 nm for the starting silicon wafer, 1.44 nm for the sol–gel TiO_x layers, and 1.7 nm for the control TiO_x based on a 1 μm × 1 μm scan of the substrate. The silane layers, on the other hand, have very different and high roughness with: sample ($-CF_3$) 3.9 nm, sample benzophenone 2.3 nm, sample ($-CH_3$) 2.7 nm, and sample ($-NH_2$) 2.9 nm for the sol–gel TiO_x. Note that the roughness in this scale is independent of the average thickness as measured by ellipsometry, which measures over the laser spot size in mm^2 as compared to what is observed in a 1000th smaller 1 μm × 1 μm area of the AFM image. It is clear that after silanization, the surfaces did not exhibit a very uniform and ideal morphology. Such surfaces are usually found only with the use of very flat mica or crystalline Au substrates, which are not sufficient for oxide surface comparison.

3.4. Protein adsorption studies

Initially, the non-specific adsorption of serum albumin of silanized sol–gel TiO_x and control TiO_x–Ti/Si-wafer was investigated and monitored by changes in the contact angle and thickness. For the sol–gel TiO_x, the measured contact angles of the samples are shown in Table 4. The ellipsometric thickness data are summarized in Table 5. After protein adsorption,

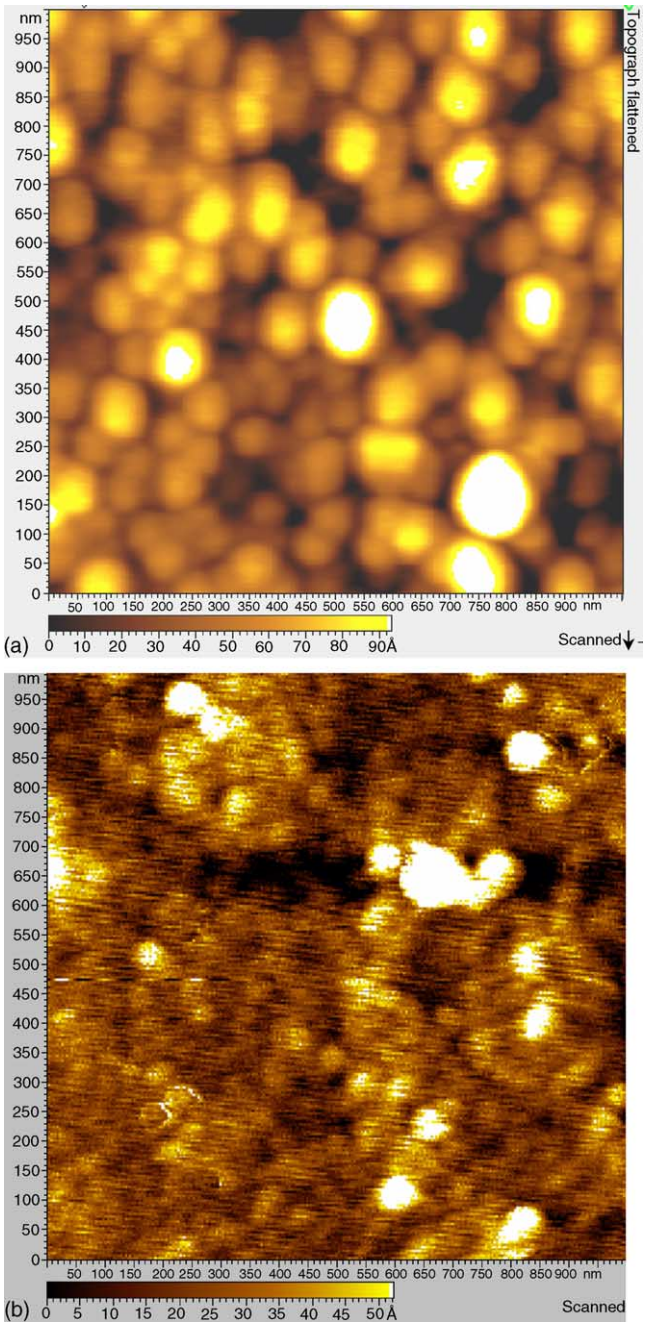

Fig. 3. (a) AFM image of control TiO_x/Ti–Si-wafer oxide surface after piranha solution treatment, (b) AFM image of oxide surface of the sol–gel TiO_x layer prior to SAM modification. A 1 μm × 1 μm images using MAC mode.

the water contact angles of both samples decreased indicating adsorption of the protein. For the TiO_x–sol–gel/SiO_x–Si-wafer, the lowest contact angle (most hydrophilic) surface was on samples (–NH_2) and benzophenone ($p = 0.103$) and the highest on the least hydrophilic samples (–CF_3) and (–CH_3) with $p = 0.980$. The average thickness of protein deposited was similarly highest on samples benzophenone and (–CH_3), while the least is on sample (–CF_3). For the control TiO_x/Ti-Si-wafer, the contact angles followed the trend on

Table 4
Water contact angle after albumin adsorption

	TiO_x–sol–gel on SiO_x–Si-wafer mean (S.D.)	Control–evaporated TiO_x–Ti/Si-wafer mean (S.D.)
–CF_3	75 (5)	82 (2)
–CH_3	74 (5)	68 (2)
–NH_2	66 (5)	54 (2)
Benzophenone	69 (5)	62 (2)

sol–gel which is dependent on the chemistry of the silanes deposited underneath. But the thickness of adsorbed protein was different, where sample (–NH_2) was thicker on the control compared to the sol–gel ($p < 0.05$) and the protein adsorbed on (–CF_3) was thicker on modified sol–gel compared to the control ($p < 0.05$). On the other hand, the thickness of the adsorbed proteins on samples benzophenone and (–CH_3) were not significantly different for both substrates ($p = 0.075$).

To compare the effect of morphologies, protein adsorption was first made on the sol–gel TiO_x and the control TiO_x/Ti–Si-wafer without the silane modification. From the AFM images, the morphology and the roughness of sol–gel coated and vacuum deposited substrates were not significantly different after protein adsorption (Fig. 6). However, the average rms roughness after protein adsorption was higher in sol–gel derived TiO_x (4.4 nm) than on the control TiO_x–Ti/Si-wafer (1.8 nm). The ellipsometric thickness data after protein adsorption on silanized surfaces are summarized in Table 4. In general, the thickness of the adsorbed proteins on the sol–gel TiO_x layers is greater than the control TiO_x. Thicker layers were observed on samples benzophenone and (–CH_3) and the least on sample (–CF_3). For the control TiO_x–Ti/Si-wafer, the highest thickness was observed on sample (–NH_2), followed by sample (benzophenone) and the least on samples (–CF_3) and (–CH_3). The surface morphologies of sol–gel derived TiO_x is shown in Fig. 7. The surfaces were uniform on larger scans of 10 μm × 10 μm but non-homogeneous at the submicron range. Samples (benzophenone) and (–CH_3) were more patchy in appearance. For the control TiO_x, sample (–NH_2) had a very different morphology compared to the other substrates as shown in Fig. 8. Samples (–CF_3), (benzophenone) and (–CH_3) consist of closely packed spherical domains while sample (–NH_2) was more flat and patchy.

The rms roughness was 5.8, 6.2, 3.3, and 5.9 nm for samples (–CF_3), –(CH_3), (–NH_2), and benzophenone re-

Table 5
Thickness of albumin after adsorption mean (S.D.)

	TiO_x–sol–gel on SiO_x–Si-wafer mean (S.D.)	Control–evaporated TiO_x–Ti/Si-wafer mean (S.D.)
–CF_3	1.58 (0.04)	0.28 (0.13)
–CH_3	2.65 (0.29)	0.50 (0.13)
–NH_2	2.07 (0.23)	4.10 (0.21)
Benzophenone	2.53 (0.37)	1.97 (0.18)

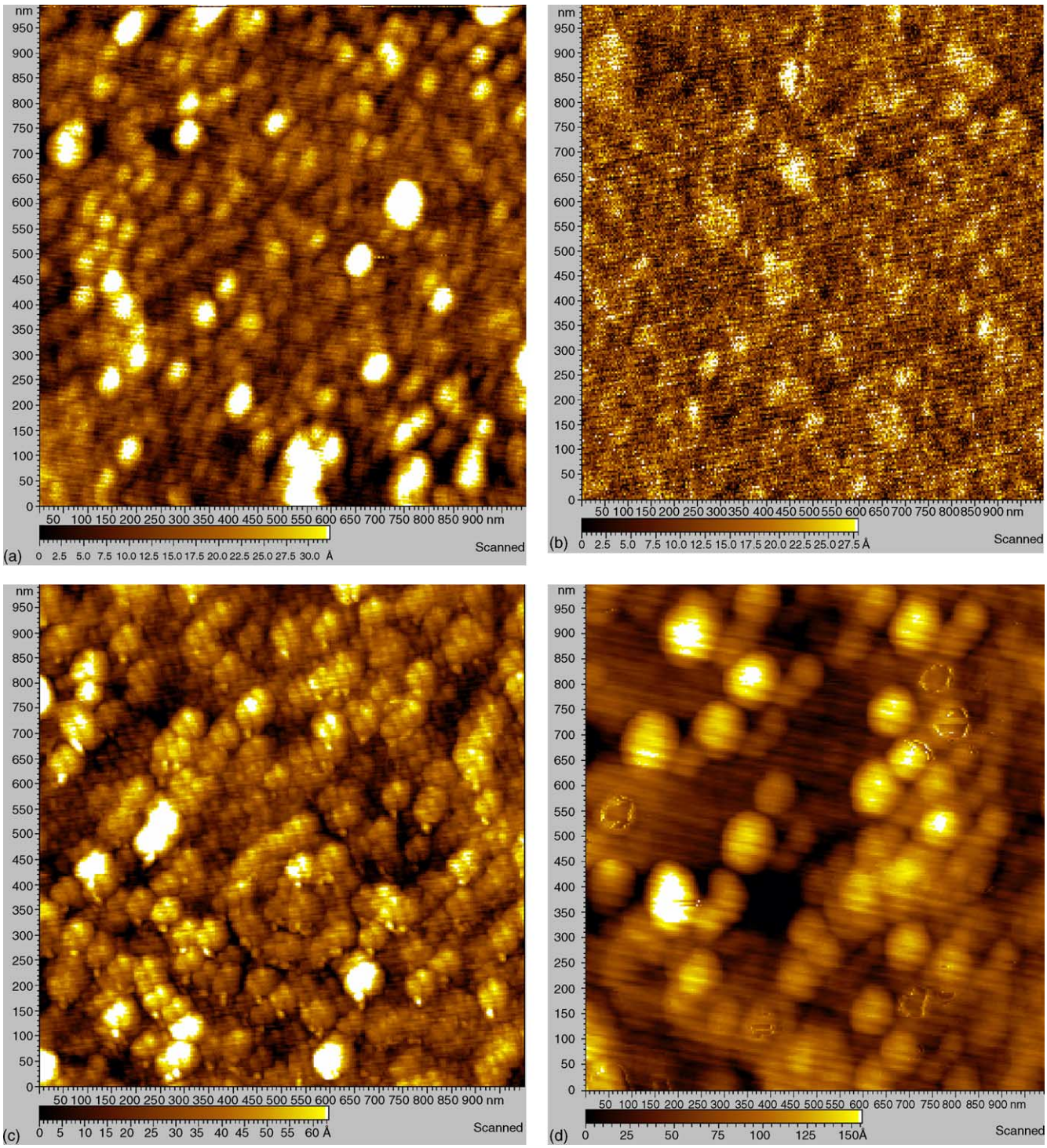

Fig. 4. The SAM formation on the sol–gel prepared TiO_x for (a) $-CF_3$, (b) benzophenone, (c) $-CH_3$, and (d) $-NH_2$. A 1 μm × 1 μm images using MAC mode.

spectively. Again, the roughness in this scale is independent of the average thickness as measured by ellipsometry, which measures over the laser spot size in mm^2 as compared to what is observed in a 1 μm × 1 μm in this scale.

The BSA protein surface coverage on the silanized sol–gel surfaces was estimated using a formula previously determined [14]. The constants and values used in the formula were in accordance with studies investigating the non-specific adsorption of albumin [14,21]. The surface coverage is shown in Fig. 9. This indicates a higher coverage of protein adsorbed on sample benzophenone and sample ($-CH_3$) in congruence with optical thickness measurements while the least was on sample ($-CF_3$). The adsorbed mass ranged from 0.2 to 0.3 μg/cm^2. In the case of control TiO_x, the adsorbed

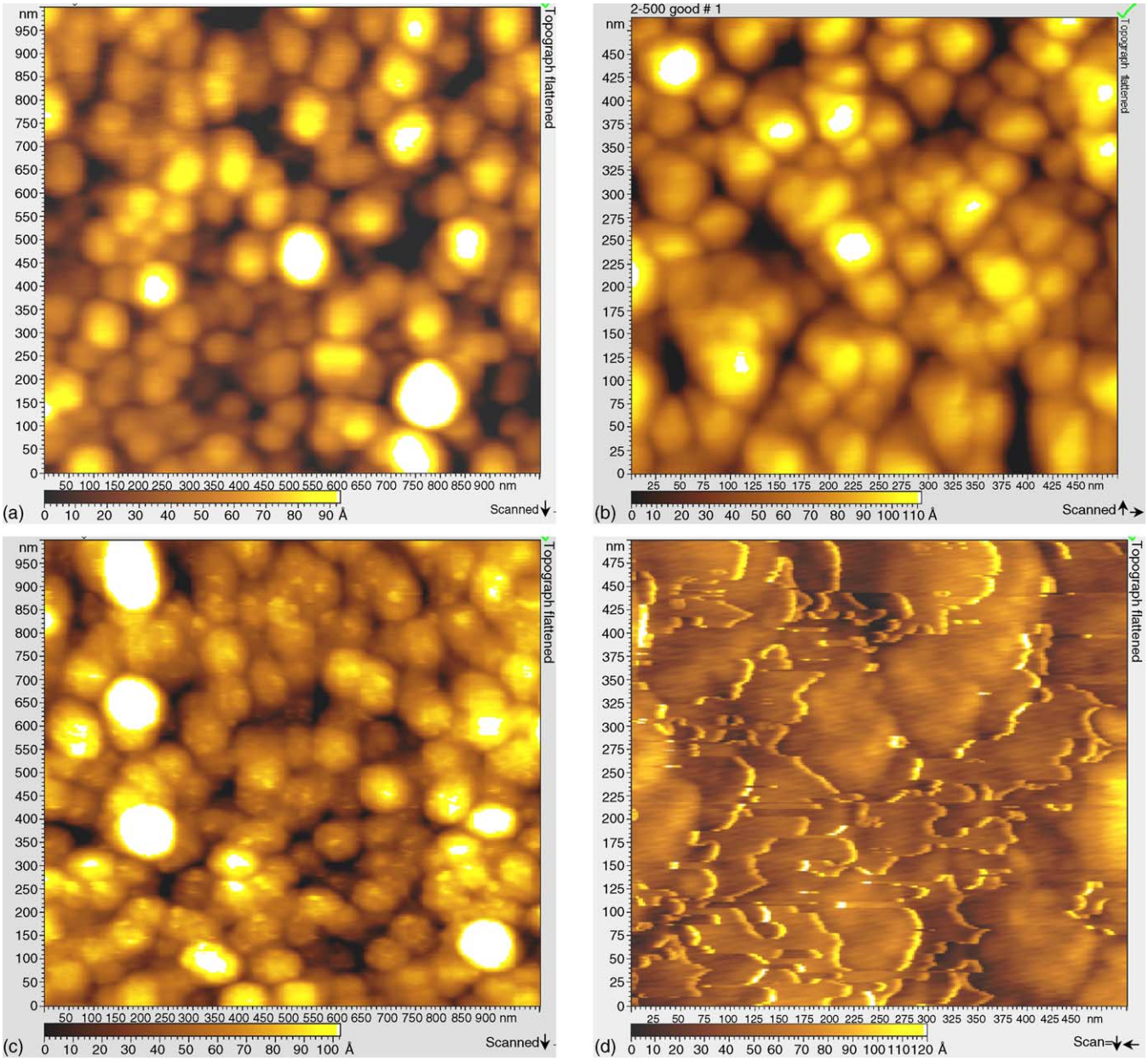

Fig. 5. The SAM formation on the TiO_x/Ti–Si-wafer control substrate (vacuum evaporated) for (a) $-CF_3$, (b) benzophenone, (c) $-CH_3$, and (d) $-NH_2$. A 1 μm × 1 μm images using MAC mode.

mass of albumin for the different SAMS ranged from 0.05 to 0.5 μg/cm^2. The highest BSA surface coverage was on sample $-NH_2$ while the least is on sample ($-CF_3$). This indicates that the sol–gel treated samples in general gave higher protein surface concentrations while the control-TiO_x SAMs can give either very low or very high adsorbed protein concentrations.

Clearly, the differences in wettability and thickness after protein adsorption were also consistent with the chemistry of the layers. For instance, the thickness of sample ($-NH_2$) on control-TiO_x can be attributed to the presence of amino groups which promotes the adsorption of albumin regardless of the underlying substrate. In addition, secondary reactions of silane with the amino group and self-crosslinking to form aggregates can contribute to this better wettability [24]. The surface morphology after protein adsorption consists of amorphous spherical domains that have also been demonstrated in previous adsorption studies of serum albumin [26]. In the presence of silane layers, the contact angle of the surfaces and roughnesses after protein adsorption varied. Without the presence of silanes, the AFM images and roughness of sol–gel coated and vacuum deposited substrates were not significantly different after protein adsorption. This indicates that the protein could adsorb through different modes other than electrostatic attraction and with different morphologies. It also indicates the crucial effect of the SAM surface modification step even for the sol–gel derived coatings, i.e. the last

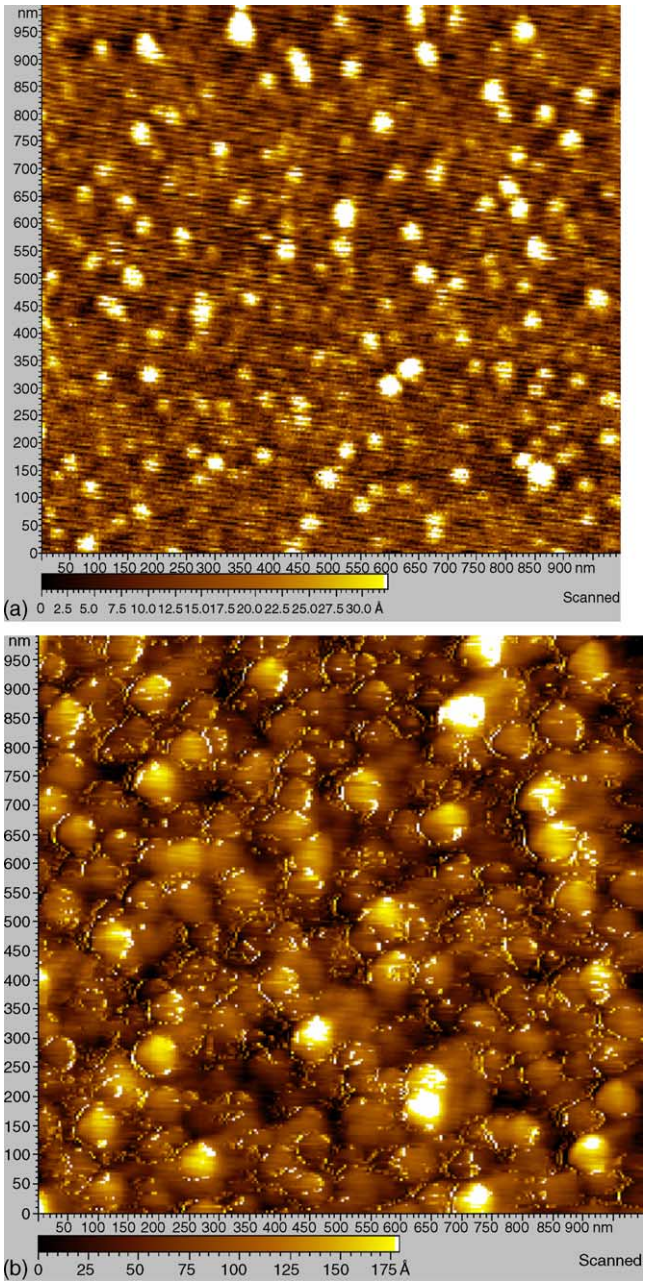

Fig. 6. BSA protein adsorption on the (a) sol–gel prepared TiO_x and (b) vacuum deposited TiO_x/Ti–Si-wafer control substrates. A 1 μm × 1 μm images using MAC mode.

layer of the SAM plays a dominant role in the adsorption, regardless of the morphology of the underlying layers.

The adsorbed mass of albumin on all silane surfaces was greater than the theoretical values assuming either a close-packed monolayer or a random sequential adsorption (RSA) model [23]. A possible explanation for the higher saturation values compared to the theoretical values is the surface diffusion of the macromolecules, allowing reorganization of the randomly adsorbed proteins into a more tightly packed layer [23]. In addition, the highest surface concentrations were found on surfaces with higher roughness after protein adsorption indicating that surface topography could also be responsible together with a higher surface area in a rougher morphology. The structural rearrangement of protein molecules during the slow adsorption process as the serum protein binds to the oxidized surface should also be considered [27].

3.5. XPS investigation

By XPS, the elemental composition (expressed in atomic percent) of Ti, Si, O, and C on the different substrates can be determined as shown in Table 6. TiO_x (Ti 2p) peak at 459 eV was found in both the vacuum deposited TiO_x/Ti control and sol–gel TiO_x substrates. Elemental Ti was only detected on vacuum deposited samples (453.8 eV). Peak analysis of O (not shown) revealed predominantly adsorbed water on vacuum deposited substrate and oxides (OH^-, CO_3^-) on the sol–gel TiO_x layer. The binding energy of O occurred at 529.5 eV which was assigned to TiO_2, and 533 eV which is due Ti–OH groups. Binding energies of Si were observed to be present in both substrates but higher in the sol–gel TiO_x consistent with the thickness and lower density of the former [22]. Contaminants and impurities such as C, and Zn were present in small amounts. Zn contaminant was found only on the bare vacuum deposited sample. This was probably introduced through the Ti vacuum deposition process.

After protein adsorption, XPS analysis provided more evidence of the presence of proteins on the substrate surface (Fig. 10). The atomic concentration of N, C and O and N relative to Ti is shown in Table 6. A higher Na contaminant was observed on the protein adsorbed samples. Na contaminant can also be introduced from the phosphate buffer solution. Zn contaminant was not detected this time. Peak fit of C 1s shows that the typical C environments are present on the sample surface: C–C, C–H, C–O, C=O, CN, CO_3. The presence of carboxylic groups confirms the deposition of organic material. N 1s at ~401 eV is typical of N in organic matrix (C–N). S 2p signals are very weak and therefore the quantification figures have large errors. The presence of strong Si 2p signals on sol–gel TiO_x samples indicates less dense and porous coverage on Si/SiO_x substrate. The N:Ti atomic ratio was 53% for vacuum deposited TiO_x/Ti, while it was 80% for the sol–gel TiO_x layer which indicate greater protein deposition on the latter oxide layer. No XPS data is available at present for silanized samples. Further XPS measurements will be made on the different SAMs with adsorbed BSA.

In general, the XPS analysis indicated clear differences on the oxide layer preparation and composition. The TiO_x gel layer was predominantly TiO_2. However, higher elemental Ti was present on the vacuum sample obviously due to the pure titanium deposited by this method. While the sol–gel is homogeneously composed of Ti, there was a higher concentration of hydroxides. Depth profile analysis of the film may reveal more information about the chemistry of the film. The persistent and strong signals from Si especially in the sol–gel samples indicated two things: (1) incomplete coverage of the

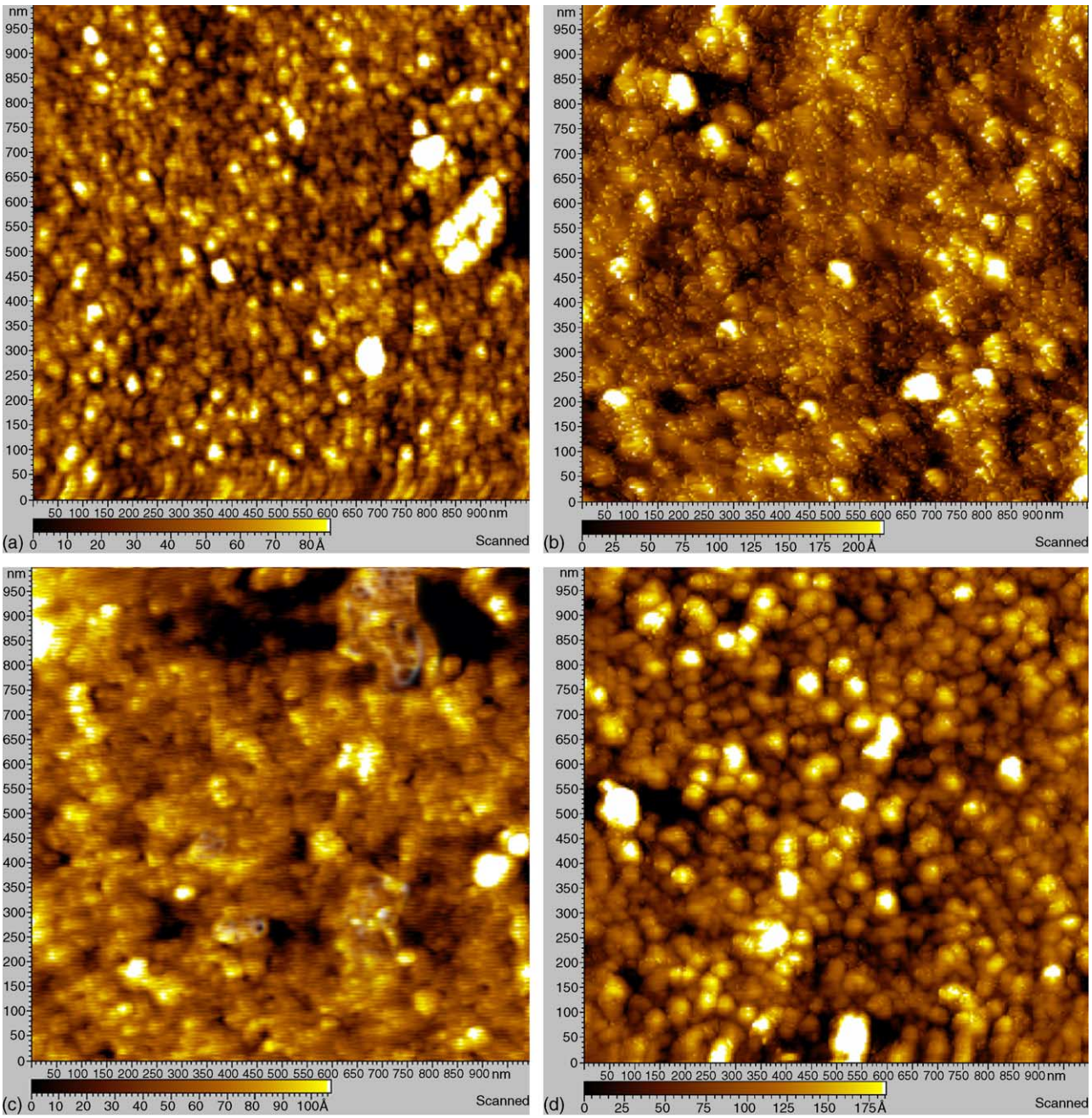

Fig. 7. BSA protein adsorption on the sol–gel prepared TiO_x substrate with SAM modification for (a) $-CF_3$, (b) benzophenone, (c) $-CH_3$, and (d) $-NH_2$. A 1 μm × 1 μm images using MAC mode.

Table 6
Atomic concentration (%) by XPS with reference to C 1s BE at 285 eV

XPS signals/peaks (eV)	TiO_x/Ti (C)	TiO_x/Si (SG)	Prot. TiO_x/Ti (C)	Prot. TiO_x/Si (SG)
O 1s (532.5)	57.96	45.63	49.04	40.57
Ti 2p (458.7)	19.01	13.05	12.84	9.73
Si 2p (103.0)	3.00	12.16	–	–
C 1s (284.5)	3.03	2.91	29.81	35.98
Zn 2p (1021)	4.02	–	–	–
N 1s (398.9)	–	–	6.84	7.74
S 2p (162.7)	–	–	0.02	0.6
Na 1s (1072)	–	–	1.4	0.5

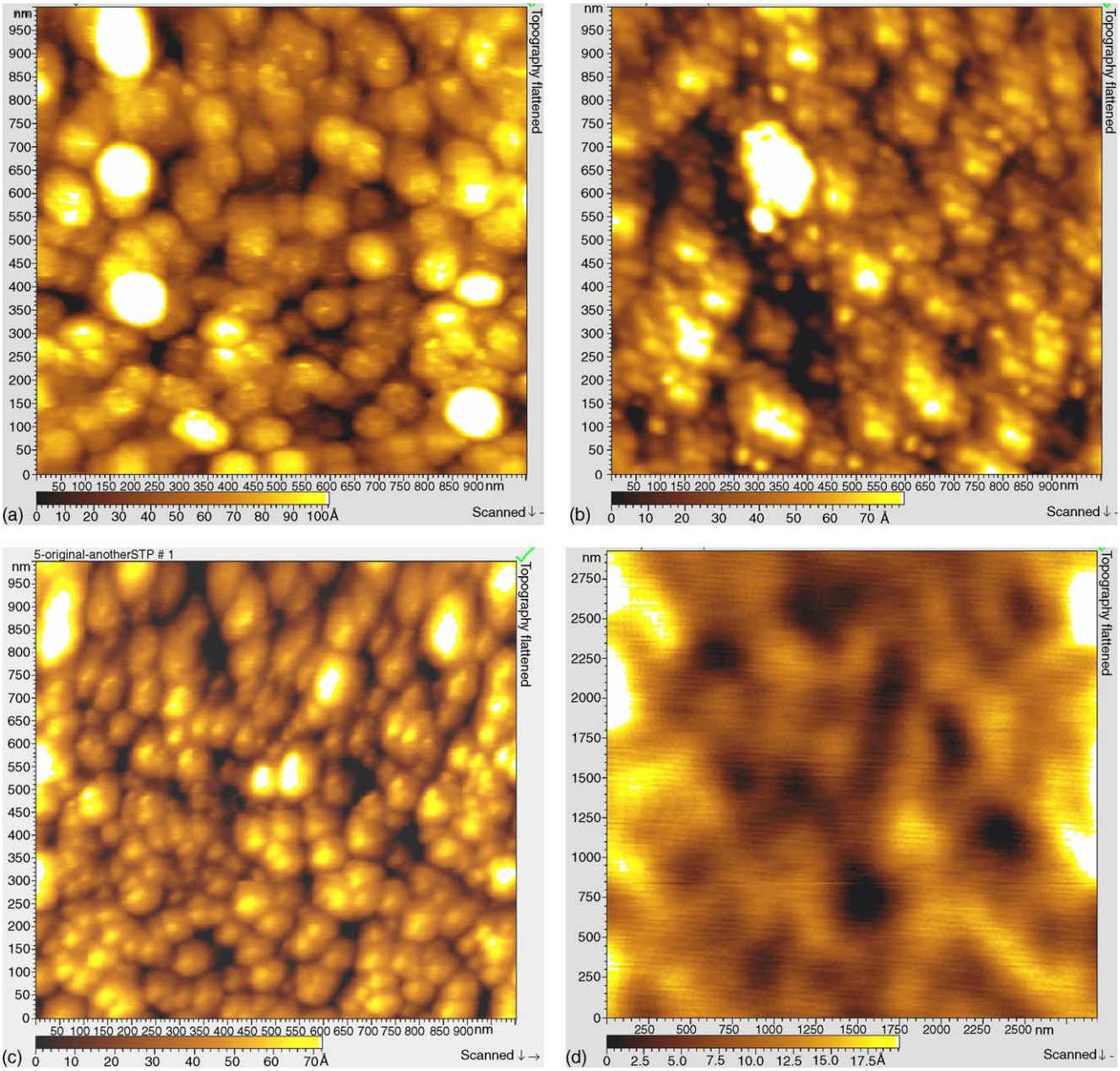

Fig. 8. BSA protein adsorption on the vacuum deposited TiO_x/Ti–Si-wafer control substrates with SAM modification for (a) $-CF_3$, (b) benzophenone, (c) $-CH_3$, and (d) $-NH_2$. A 1 μm × 1 μm images using MAC mode.

Si substrate because of the porosity, and given the thickness of the overlaying silane (2) the penetration depth of the XPS is sensitive to the underlying Si-wafer. After protein adsorption, XPS analysis of the samples indicated conclusively the presence of proteins on the substrate surface (Fig. 9). Peak fit of C 1s and N 1s (not shown) revealed the typical C environments are present on the sample surface: C–C, C–H, C–O, C=O, CN, CO_3, which confirms the presence of organic moieties. The N:Ti atomic ratio was 53% for vacuum deposited TiO_x/Ti, while it was 80% for the sol–gel TiO_x layer despite a higher overlayer of C 1s. These results indicated that the composition of the sol–gel oxide was similar to the native oxide. Contaminants in very low intensities were not considered undesirable as the amorphous native oxide of titanium has been shown to contain carbon-dominated contaminants and trace amounts of N, Ca, P, Cl, S, Na and Si [11,28]. Further XPS measurements will be made on the different SAMs with adsorbed BSA.

3.6. Future studies

SAMs have been used to immobilize streptavidin and biotinylated DNA on sol–gel silicon oxide and investigated by surface plasmon spectroscopy [13]. Again, studies have

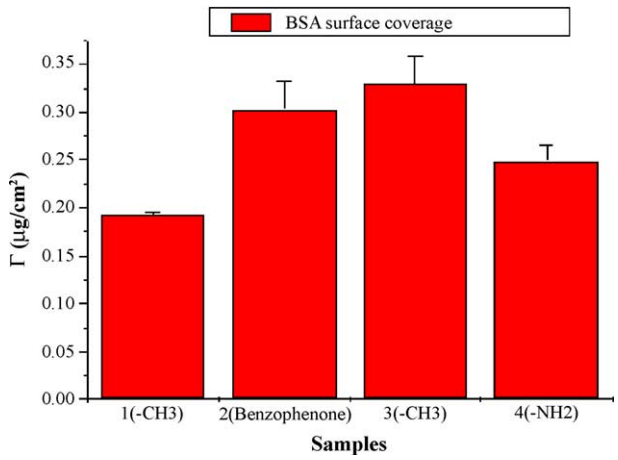

Fig. 9. Surface coverage of adsorbed bovine serum albumin (BSA) on silanized sol–gel substrates. Mean value plus standard error.

been made on ideal surfaces of mica and Au, modified with SAMs. However, oxide surfaces are generally more corrugated in their morphology compared to these ideal substrates. To our knowledge though, this is the first time that SAMs have been deposited on top of sol–gel derived TiO_x by this surface sol–gel processing technique and the protein adsorption investigated systematically. Furthermore, the effect of the surface properties such as topography, wettability, surface chemistry and oxide thickness of these modified titanium surfaces on adsorption in vitro of protein were investigated. We are currently investigating control of the surface properties of metallic implants such as titanium alloys for example using this surface sol–gel method. It is well known that exposed surfaces of titanium metal alloys are spontaneously covered by a passive 3–6 nm layer of native noncrystalline TiO_x [11]. However, these alloys also have unpredictable biocorrosion properties. This could affect the adsorption of serum proteins and ability of the surface to form bone. By modifying such substrate with a sol–gel TiO_x layer, it should be possible to passivate the surface more uniformly. The results presented in this study may be useful in controlling the non-specific adsorption of proteins. The titanium surface may be modified to enhance or resist the adsorption of albumin (a non-adhesive protein to osteoblast cells) and will be useful in the design of implants that both contact bone and smooth muscle tissue. Thus, an important outcome of this study is its possible application to titanium and titanium alloy bioimplant modification.

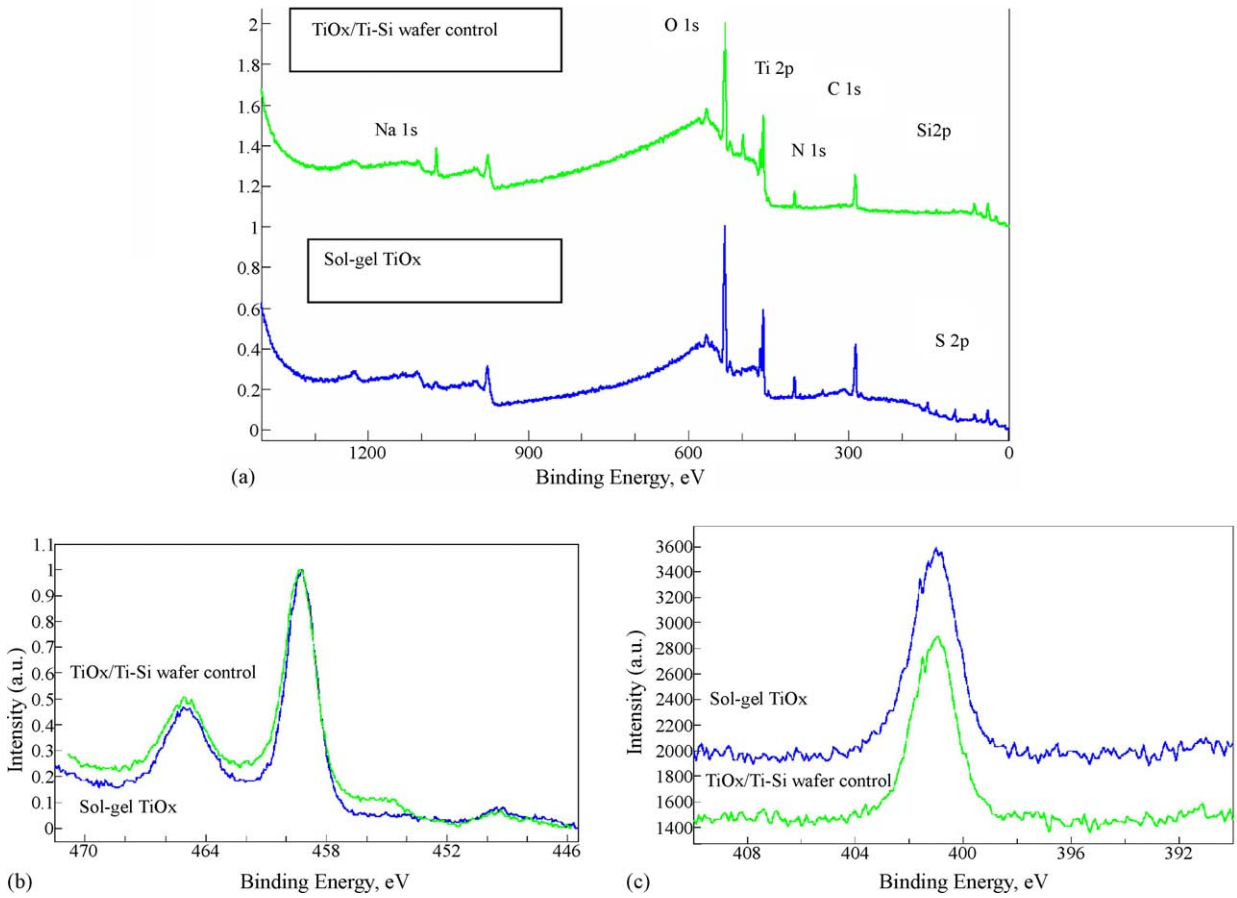

Fig. 10. XPS scans: (a) XPS survey scan after BSA protein adsorption on TiO_x/Ti–Si-wafer vacuum deposited and sol–gel TiO_x, (b) TiO_x 2p (458.7) and (c) N 1s (400.9) high resolution scans.

4. Conclusions

Our results showed the effect of sol–gel processing and SAM modification on the non-specific adsorption of proteins. In addition, this study showed subtle differences in surface properties and in vitro effects on protein behavior of TiO_x films prepared by conventional vacuum deposition and surface sol–gel process. The rough surface morphology primarily determined the thicker SAM formation and at the same time influenced higher protein adsorption. On the other hand, the trends on the surface energy of the SAMs (hydrophobic or hydrophilic) are consistent regardless of the underlying oxide layer. Furthermore, in the absence of the SAMs, there is no observable difference in the protein adsorption behavior between the two oxides. Thus, the study confirms that the surface sol–gel is an effective alternative method to synthesize TiO_x layers with precise nm thickness. Sol–gel processing has the advantage of precise control of the nanostructure and thickness of these ultrathin coatings. Surface modification of sol–gel derived TiO_x by SAMs may further influence in vitro protein adsorption due to changes in the chemical composition of the surface, wettability and roughness. There is a need to confirm any protein specificity on the TiO_x gel surfaces by SAMs through the use of other protein derivatives, e.g. RGD specific, and other surface sensitive spectroscopic and microscopic analysis. In addition, the effect of surface chemistry, composition, and topography of these films on osteoblast differentiation and mineralization should be investigated and compared with TiO_x surfaces produced by conventional methods.

Acknowledgments

We would like to acknowledge funding from NSF DMR-0315565 and technical support from Molecular Imaging Inc. and Optrel GmBH and the staff of the Department of Chemistry, University of Alabama at Birmingham.

References

[1] M.A. Schwartz, M.D. Schaeller, M.H. Ginsberg, Integrins: emerging paradigms of signal transduction, Annu. Rev. Cell. Dev. Biol. 11 (1995) 549–599.
[2] D.A. Puleo, R. Bizios, Mechanisms of fibronectin-mediated attachment of osteoblasts to substrates in vitro, Bone Mier. 18 (3) (1992) 215–226.
[3] A. Klinger, D. Steinberg, D. Kohavi, M.N. Sela, Mechanism of adsorption of human albumin to titanium in vitro, J. Biomed. Mater. Res. 36 (3) (1997) 387–392.
[4] B. Kasemo, J. Lausmaa, Biomaterial and implant surface: a surface science approach, Int. J. Oral. Maxillofac. Implants 3 (1988) 83–101.
[5] D. Deligianni, N. Katsala, S. Ladas, D. Sotiropoulou, J. Amedee, Y. Missirlis, Effect of surface roughness of the titanium alloy Ti_6Al_4V on human bone marrow cell response and on protein adsorption, Biomaterial 22 (2001) 1241–1251.
[6] K. Healy, C. Thomas, A. Rezania, J. Kim, P. McKeown, B. Lom, P. Hockberger, Kinetics of bone cell organization and mineralization on materials with patterned surface chemistry, Biomaterials 17 (1996) 195–208.
[7] K. Kilpadi, P. Chang, S. Bellis, Hydroxylapatite binds more serum proteins, purified integrins, and osteoblast precursor cells than titanium or steel, J. Biomed. Mater. Res. 57 (2001) 258–267.
[8] H.B. Wen, Q. Liu, J. de Wijn, K. de Groot, Preparation of bioactive microporous titanium surface by a new two step chemical treatment, J. Mater. Sci.: Mater. Med. 9 (1998) 121–128.
[9] K. Acharya, T. Kunitake, A general method for fabrication of biocompatible surfaces by modification with titania layer, Langmuir 19 (2003) 2260–2266.
[10] E. Gawalt, M. Avaltroni, N. Koch, J. Schwartz, Self assembly and bonding of alkanephosphonic acids on the native oxide surface of titanium, Langmuir 17 (2001) 5736–5738.
[11] A. Nanci, J.D. Wuest, L. Peru, P. Brunet, V. Sharma, S. Zalzal, M.D. Mckee, Chemical modification of titanium surfaces for covalent attachment of biological molecules, J. Biomed. Mater. Res. 40 (1998) 324–335.
[12] A. Rezania, R. Johnson, A. Lefkow, K. Healy, Bioactivation of metal oxide surfaces. 1. surface characterization and cell response, Langmuir 15 (1999) 6931–6939.
[13] D. Kambhampati, T. Jakob, J. Robertson, M. Cai, J. Pemberton, W. Knoll, Langmuir 17 (2001) 1169–1175.
[14] M. Lestelius, B. Liedberg, P. Tengvall, In vitro plasma protein adsorption on ω-functionalized alkanethiolate self-assembled monolayers, Langmuir 13 (1997) 5900–5908.
[15] C. Jenney, K. Defifie, E. Colton, J. Anderson, Human monocyte/macrophage adhesion, macrophage motility, and IL-4 induced foreign body giant cell formation on silane-modified surface in vitro, J. Biomed. Mater. Res. 41 (1998) 171–184.
[16] K. Webb, V. Hlady, P. Tresco, Relationships among cell attachment, spreading, cytoskeletal organization, and migration rate for anchorage-dependent cells on model surfaces, J. Biomed. Mater. Res. 49 (2000) 362–368.
[17] P. Filippini, G. Rainaldi, A. Ferrante, B. Mecheri, G. Gabrielli, M. Bombace, P. Indovina, M. Santini, Modulation of osteosarcoma cell growth and differentiation by silane-modified surfaces, J. Biomed. Mater. Res. 55 (2001) 338–349.
[18] Q. Liu, J. Ding, F. Mante, S. Wunder, G. Baran, The role of surface functional groups in calcium phosphate nucleation on titanium foil: a self-assembled monolayer technique, Biomaterials 23 (2002) 3103–3111.
[19] I. Ichinose, H. Senzu, T. Kunitake, Stepwise Adsorption of metal alkoxides on hydrolyzed surfaces: a surface sol–gel process. Chem. Lett. 1996.
[20] N. Kovtyukhova, E. Buzaneva, C. Waraksa, T. Mallouk, Ultrathin nanoparticle ZnS and ZnS:Mn films: surface sol–gel synthesis, morphology, photophysical properties, Mater. Sci. Eng. B 69–70 (2000) 411–417.
[21] T. Ito, Y. Okayama, S. Shiratori, The fabrication of organic/inorganic multilayer by wet process and sequential adsorption method, Thin Film Solids 393 (2001) 138–142.
[22] M. Fang, C.H. Kim, B.R. Martin, T.E. Mallouk, Surface sol–gel synthesis of ultrathin titanium and tantalum oxide films, J. Nanoparticle Res. 1 (1999) 43–49.
[23] F. Hook, J. Voros, M. Rodahl, R. Kurrat, P. Boni, J. Ramsden, M. Textor, N. Spencer, P. Tengvall, J. Gold, B. Kasemo, A comparative study of protein adsorption on titanium oxide surfaces using in situ ellipsometry, optical waveguide lightmode spectroscopy and quartz crystal microbalance/dissipation, Colloids Surf. B: Biointerf. 24 (2002) 155–170.
[24] A. Fadeev, T. McCarthy, Self-assembly is not the only reaction possible between alkyltrichlorosilanes and surfaces: monomolecular and oligomeric covalently attached layers of dichloro and trichlorosilanes on silicon, Langmuir 16 (2000) 7268–7274.

[25] D. Li, M. Lütt, M. Fitzsimmons, R. Synowicki, M. Hawley, G. Brown, Preparation, characterization, and properties of mixed organic and polymeric self-assembled multilayers, J. Am. Chem. Soc. 120 (1998) 8797–8804.
[26] J. Fang, C. Knobler, Phase-separated two-component self-assembled organosilane monolayers and their use in selective adsorption of a protein, Langmuir 12 (1996) 1368–1374.
[27] A. Valagao Amadeu do Serro, A. Fernandes, B. Saramago, W. Norde, Bovine serum albumin adsorption on titania surfaces and its relation to wettability aspects, J. Biomed. Mater. Res. 46 (1999) 376–381.
[28] M. Esposito, J. Lausmaa, J. Hirsch, P. Thomsen, Surface analysis of failed oral titanium implants, J. Biomed. Mater. Res. (Appl. Biomater.) 48 (1999) 559–568.